Fuel Processing Technology 248 (2023) 107827

Contents lists available at ScienceDirect

Fuel Processing Technology

journal homepage: www.elsevier.com/locate/fuproc

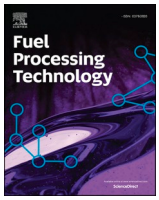

Plasma assisted dry reforming of methane: Syngas and hydrocarbons formation mechanisms

Paula Navascués [a,*], José Cotrino [a,b], Agustín R. González-Elipe [a], Ana Gómez-Ramírez [a,b,*]

[a] Laboratory of Nanotechnology on Surfaces and Plasma, Instituto de Ciencia de Materiales de Sevilla (CSIC-Universidad de Sevilla), Avda. Américo Vespucio 49, E-41092 Seville, Spain
[b] Departamento de Física Atómica, Molecular y Nuclear, Universidad de Sevilla, Avda. Reina Mercedes, E-41012 Seville, Spain

ARTICLE INFO

Keywords:
Methane dry reforming
Hydrogen production
Packed-bed plasma reactor
Isotope labeling
Plasma-catalysis
Plasma-assisted processes

ABSTRACT

Plasma reactions of CO_2 + CH_4 mixtures have been proposed as a suitable process for the dry reforming of methane. Without specific catalysts, most studies report the formation of CO and H_2 as main reaction products and arise the question whether CH_x radicals coming from CH_4 may interact with intermediate species formed by electron impact dissociation of CO_2, a critical step for the formation of high added value oxygenated compounds. We have addressed this question studying the CO_2 + CH_4 plasma reaction in a ferroelectric-moderated packed-bed reactor varying the reactants ratio. Analysis of the reaction products by mass spectrometry and the plasma reaction intermediates by optical emission spectroscopy suggest that few direct cross-link interactions exist between intermediate plasma species issued from CH_4 or CO_2. This preliminary evidence is corroborated by experiments using $^{13}CO_2$ instead $^{12}CO_2$ as reactant. The isotope labeling procedure has proved that plasma reaction mechanisms of CO_2 and CH_4 molecules proceed almost independently, with the formation of small amounts of water and the removal of carbon deposits resulting CH_4 plasma decomposition as sole evidences of cross reactions. These results highlight the need of using catalysts to promote specific surface reactions for a better control of the selectivity of the process.

1. Introduction

Due to its high hydrogen content, methane (CH_4) is frequently used as a feedstock in the chemical industry and as a fuel with relatively low environmental impact. However, the high volatility of this gas dissolved in crude oils makes that around 8% of methane becomes directly released to the atmosphere during shale gas extraction and distribution [1], thus intensively contributing to the global warning [2]. Avoiding these wastes and transforming methane into higher added value compounds (e.g., hydrogen, organic oxygenates or C_n unsaturated hydrocarbons) is important both from a societal point of view and to provide suitable and manageable reactants to the chemical industry [3,4]. A quite attractive process for this purpose is the reaction between CH_4 and CO_2, the two main gases responsible for the greenhouse effect affecting our planet and where the latter might act as CO source and/or to supply the oxygen required for the formation of oxygenated products. In the chemical industry, the direct reaction of CH_4 with CO_2, generally recognized as the dry reforming of methane (DRM), renders *syngas* (i.e., a mixture of CO and H_2) as typical reaction output [5] usable as fuel or as a raw mixture for the synthesis of other valuable chemicals. The reaction of CH_4 and CO_2 at high temperatures, while resulting effective for *syngas* production, it is not useful for the production of oxygenates or other high-added value carbon compounds because these products may readily decompose or recombine at high temperatures [6].

Alternatively to thermal catalytic reactions, the non-thermal plasma reaction of CH_4 + CO_2 mixtures has conceited much interest during the last few years [5,7–11], particularly when carried out by means of the so-called dielectric barrier discharge reactors (DBD) [12–15], either with or without catalysts, in a packed-bed reactor configuration. In general, *syngas* is the main reaction product obtained in these plasma reactors although C_n hydrocarbons ($n > 1$) can also be obtained [5]. This large variety of possible products, the limited control of the CO/H_2 ratio in the obtained *syngas-like* mixture and a low selectivity towards a specific hydrocarbon or oxygenated product still preclude a profitable use of CH_4 + CO_2 plasma reactions. Moreover, from a methodological point of view, a poor control on selectivity imposes some restrictions for a

* Corresponding authors at: Laboratory of Nanotechnology on Surfaces and Plasma, Instituto de Ciencia de Materiales de Sevilla (CSIC-Universidad de Sevilla), Avda. Américo Vespucio 49, E-41092 Seville, Spain.
E-mail addresses: paula.navascues@icmse.csic.es (P. Navascués), anamgr@us.es (A. Gómez-Ramírez).

https://doi.org/10.1016/j.fuproc.2023.107827
Received 4 November 2022; Received in revised form 12 April 2023; Accepted 5 May 2023
Available online 11 May 2023

proper analysis of the process energetics, which is generally discussed in terms of *syngas* formation [5], i.e., assuming that this reaction mixture is majority and therefore disregarding the formation of other compounds. Nevertheless, the formation of C_n hydrocarbons in these processes suggests that plasma reactions such as $nCH_4 \rightarrow C_nH_y + (4n\text{-}y)/2\ H_2$ may constitute a significant source of hydrogen [16–18]. This also suggests that CO* and O* plasma species stemming from CO_2 dissociation [5] do not massively interact in the plasma either with CH_4 or with CH_x* ($x < 4$) intermediate species, the latter likely formed by plasma electron impact dissociation of methane [19]. Such a direct interaction would be required for the formation of oxygenated compounds as reaction products [3,20,21], a process of the outmost interest for the simultaneous valorization of both CO_2 and CH_4.

Most studies about the plasma-assisted $CH_4 + CO_2$ reaction have been carried out in DBD reactors with coaxial geometries. To improve conversion rates and increase selectivity towards CO, H_2 or other compounds, a wide range of operating parameters have been varied, such as power consumption [15], gas flow rate [19,22], feed ratio [20], electrode materials [23], gap distance between electrodes [20], and the addition of inert and other gases such as Ar, He or N_2 [18,22]. A general result from these studies is that the selectivity towards hydrocarbons and H_2 formation increases and that of CO decreases with the relative amount of CH_4 in the reactant mixture [22]. It is also known that the formation of solid carbon residues detected as a byproduct of CH_4-containing plasmas tends to increase when the relative amount of CO_2 in the reactant's mixture decreases [5]. To increase the process selectivity, catalysts have been incorporated into the barrier [3]. Most commonly used catalyst formulation integrates Ni particles as active metallic phase and alumina as support [13,19,24], although particles of Pt, Cu, or Au have also been incorporated in DBD reactors [25]. Similarly, different materials have been also essayed as barriers (i.e., as discharge moderators). For example, dielectrics such as γ-Al_2O_3, ZrO_2 or SiO_2 [12], and ferroelectrics such as $BaTiO_3$ [26,27], $LaNiO_3$ [28], Barium Zirconate Titanate (BZT) and Barium Ferrite Niobate (BFN) [14]. Regarding the use of ferroelectrics, Chung et al. [14] reported that in a cylindrical packed-bed reactor BZT and BFN render higher CH_4 and CO_2 conversion rates than the reactor filled with dielectric glass beads.

On the other hand, kinetic modeling of DRM reaction mechanisms has been also attempted to elucidate the plasma-chemistry interactions in $CH_4 + CO_2$ discharges [17,29–32], although the complexity of the mixture and computational limitations has hampered the development of accurate models [5]. Despite that, a certain consensus exists in the sense that in DBD reactors CH_3* and CH_2* radicals, formed by electron impact of CH_4, may be intermediate species to eventually render C_2H_6 or C_3H_8 molecules. It is also accepted that the dissociation of CO_2 into CO and O species would be the limiting pathway for the formation of oxygenate molecules such as formaldehyde (CH_2O) or acetaldehyde (CH_3COH) through their direct interaction with methane or derived reaction intermediates [17,31]. From an experimental point of view, an intriguing issue with regard to these theoretical calculations is the fact that oxygenates are rarely formed in $CH_4 + CO_2$ plasma reactions without catalysts added and that, instead, syngas-like and C_n hydrocarbons are the majority products under most experimental conditions [5,8–10]. Interestingly, similar issues have arisen for plasma-enhanced chemical vapor deposition (PECVD) processes when analyzing gas phase and surface reactions in low-pressure [33,34] and atmospheric-pressure plasmas [35]. In these processes, the main role of oxygen atoms stemming from CO_2 dissociation [33,34] or other gas sources [35] seems to consist of the etching removal of carbon atoms formed during the film growth, instead of intervening in gas phase interactions to produce film-forming species

In the present study we have addressed some of the aforementioned questions experimentally studying $CH_4 + CO_2$ mixtures in a packed-bed plasma reactor using a bed of ferroelectric PZT pellets as moderator material. The main reaction products obtained under the selected operating conditions were H_2 + CO (i.e., *a syngas*-like mixture) plus C_n hydrocarbons, and minority amounts of H_2O. The fact that the CO/H_2 ratio varied depending on the CO_2:CH_4 inlet mixture suggests separated mechanistic routes for CO and H_2 formation. To further account for the obtained product distribution and reaction mechanisms we have used Optical Emission Spectroscopy (OES) to characterize the plasma, using for comparison the $O_2 + CH_4$ plasma reaction and applying an isotope labeling procedure using $^{13}CO_2$ instead of $^{12}CO_2$ as reactant. The application of these complementary methodologies has allowed us to experimentally demonstrate that, for the studied $CH_4 + CO_2$ mixtures and applied experimental conditions, intermediate plasma species derived from either CH_4 or CO_2 do not significantly interact in the plasma and that suitable catalysts should be incorporated into the packed-bed reactor for a tailored control of reaction selectivity.

2. Material and methods

The experiments were performed in a parallel-plate packed-bed reactor made of stainless steel (volume of 310 cm^3, inner diameter of 10.3 cm). The vessel has two electrodes of 7.5 cm in diameter made of aluminum. The grounded electrode is embedded in an insulating polymer (PEEK) to prevent sparks to the reactor chamber, which is also grounded for safer handling. The analogous upper electrode is connected to the high voltage power supply by means of an electrical feedthrough. **Fig. S1** in the supplementary material shows photographs of the reactor (also described in detail in [36,37]) and its components.

The plasma discharges were moderated with a bed of Lead Zirconate Titanate (PZT) pellets of 2–3 mm of diameter. The PZT material was supplied as powder by APC International Ltd. and were sintered as pellets in the laboratories of the Ceramic and Glass Institute (CSIC, Spain), following a procedure that can be found in previous publications of our research group [38].

The experiments were carried out at atmospheric pressure and room temperature. The reactant gas mixture was dosed into the reactor through a gridded access port located in the center of the bottom electrode, while the products and the unreacted gas mixture left the reactor chamber through two exhaust tubes connected to its upper part. To ignite the plasma, a high voltage signal was applied between the electrodes. The upper electrode was connected to a high voltage amplifier (Trek Inc. Model PD05034) coupled to an AC function generator (Stanford Research Systems, Model DS345). In this study, no strong correlation has been found between the applied voltage and the partition of reaction products in the outlet flow, and therefore the electrical parameters were optimized to maximize the flow of products (i.e., reactant conversion), fixing the frequency at 5 kHz and the voltage amplitude at 3.15 kV. A fan was used to externally cool down the reactor walls (note the maximum temperature measured at the reactor walls during operation was 40 °C). **Fig. S2** in the supplementary material illustrates a scheme of the packed-bed reactor highlighting the passage of the gases through the packed bed, as well as the electrical connections.

The applied voltage was measured using a high voltage probe connected to the active electrode, while the current was determined with a current transformer (Pearson, Current Monitor Model 6585) connected to the ground. A grounded capacitor (2.5 μF) was used to directly quantify the charge transferred through the circuit. All electrical signals were recorded with an oscilloscope (Agilent Tech., Model DSO-X 3024A). As illustrated in refs. [37, 39], the area of the Lissajous plots was taken as a measure of the consumed power by the reactor. Optical emission spectra (OES) were collected through a collimator placed at a lateral window of the reactor that was connected via an optical fiber to a spectrometer (Horiba Ltd., Jobin-Yvon FHR640). The measurements were taken using a diffraction grating centered at 330 nm that has a density of 1201 lines/cm. The resulting resolution was 0.5 nm and the integration time was set at 1 s. The reactor gas outlet was analyzed with a quadrupole mass spectrometer (QMS; Pfeiffer Vacuum, QMG 220 Prisma Plus). The products formed have been identified by comparison with the fragmentation patterns reported in the NIST Mass Spectrometer

Database [40]. **Fig. S3** in the supplementary material illustrates the connections between the reactor and all the in situ characterization techniques.

CH_4 and CO_2 have been used as reactants with a total inlet flow rate of 20 sccm. Equal or higher amounts of CH_4 with respect to CO_2 were selected to promote the formation of hydrocarbons [5]. Thus, CH_4:CO_2 feed ratios fixed at 1:1, 2:1, 3:1, and 4:1 were adjusted with mass flow controllers (Bronkhorst) set from 10 to 16 sccm and from 10 to 4 sccm for CH_4 and CO_2, respectively. Moreover, two special experiments were designed to further analyze the reaction mechanisms. A mixture of 14 sccm CH_4 and 1 sccm O_2 was ignited to study the effect of adding oxygen to a CH_4 plasma. Then, the result for the 2:1 CH_4:CO_2 mixture was analyzed applying the isotope labeling methodology, i.e., using $^{13}CO_2$ instead of $^{12}CO_2$.

To analyze the process performance, we defined the reaction yield in terms of the absolute and effective conversion rates of each reactant (i.e., CO_2 and CH_4). They are determined as follows:

$$Absolute\ Conversion\ Rate = \frac{(M(in) - M(out))}{M(in)} * 100\ (\%) \quad \text{(E1)}$$

$$Effective\ Conversion\ Rate = Absolute\ Conversion\ Rate * \frac{M(in)}{Total\ flow\ rate}\ (\%) \quad \text{(E2)}$$

where *M (in)* and *M (out)* are, respectively, the inlet and outlet gas flow rates of each reactant. The effective conversion rate *(E2)* is defined as the absolute conversion rate multiplied by the dilution of each reactant in the inlet mixture. This magnitude gives an idea on how effective the conversion of each molecule is within the boundaries of the plasma mixture. We discuss the obtained results in terms of absolute and effective rates taking into account that both magnitudes are utilized in the literature on the subject [5].

3. Results and discussion

3.1. CO_2:CH_4 ratio, reaction yield, and product selectivity

Fig. 1(a) shows the *I(t)* curves measured in stationary state conditions when varying the reactant ratio (CO_2:CH_4), while the bar plot in Fig. 1(b) shows the evolution of the power consumed by the reactor. According to Fig. 1(a), the discharges are characterized by a filamentary behavior [41], which is more prominent for the 3:1 mixture, characterized by maximum current values higher than 100 mA. Consequently, this mixture presented the highest power consumption from all the series of experiments. This also agrees with the maximum conversion rates reported below.

The CO_2:CH_4 ratio was a critical parameter controlling the reaction process either in terms of conversion rates, power consumption or products selectivity. These three aspects have been carefully analyzed in this work, keeping constant the total flow rate, the applied voltage amplitude (3.15 kV), and frequency (5 kHz). Fig. 2 shows the absolute and effective conversion rates obtained as a function of the CH_4:CO_2 ratio. According to these plots, absolute and effective CH_4 conversion rates are higher than those of CO_2 for all studied conditions. This is a first hint that CH_4 and CO_2 plasma reactions might not be interconnected as it would happen for a thermally driven reforming reaction of the type:

$$CH_4 + CO_2 \rightarrow 2CO + 2H_2 \quad \text{(E3)}$$

The highest conversion rates, 34% and 25% for CH_4, and 22% and 5.4% for CO_2, absolute and relative magnitudes, respectively, were obtained for a 3:1 ratio. As reported by many authors and according to the lower binding energy of the C—H bond (4.3 eV) than the C═O bond (8.3 eV) [3,30], the observed differences in CH_4 and CO_2 conversion rates agree with that the electron-impact excitation probability is higher for CH_4 than for CO_2 molecules.

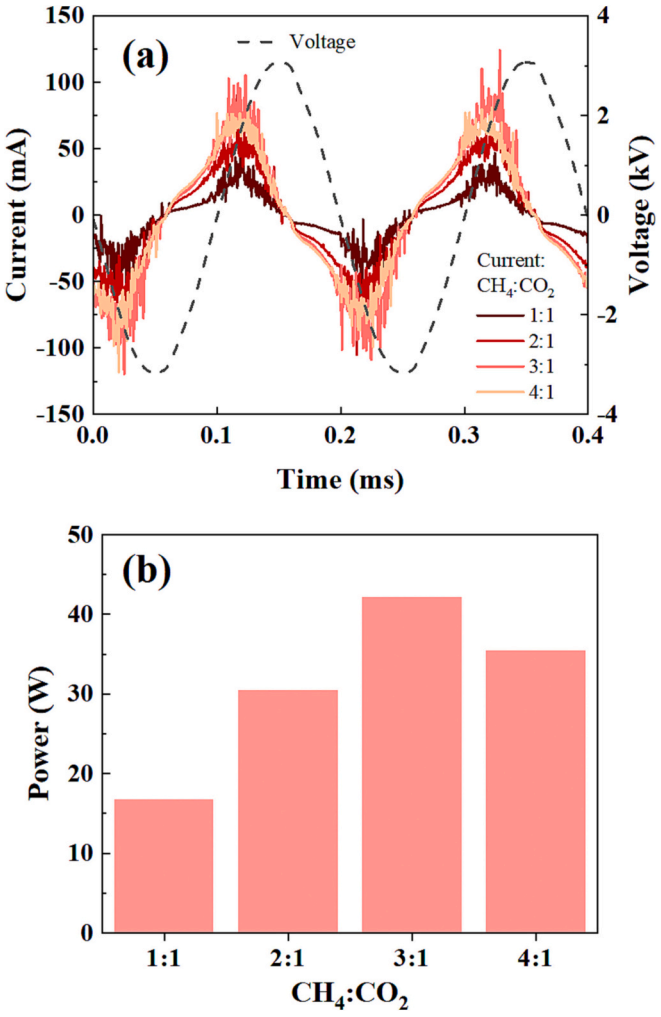

Fig. 1. Electrical characterization of the plasma reactor fed with CH_4 + CO_2 mixtures. (a) Measured current curves and (b) consumed power values as a function of the CH_4:CO_2 ratio. Operating conditions: 5 mm-PZT barrier, total flow rate of 20 sccm, voltage amplitude of 3.15 kV, frequency of 5 kHz, and CH_4:CO_2 ratio varying between 1:1 and 4:1.

The products formed upon plasma excitation of the different mixtures were analyzed by mass spectrometry. The QMS spectra obtained for the different mixtures are reported as supplementary material (**Fig. S4**). From the analysis of these spectra, it is apparent that the outlet gases detected for the different mixtures consisted of unreacted CH_4 and CO_2 and the following products: H_2 ($m/z = 2$), CO ($m/z = 28$), H_2O ($m/z = 18$), and C_2, C_3 and C_m ($m > 3$) hydrocarbons (corresponding to fragmentation patterns appearing around $m/z = 25$, $m/z = 44$ and higher m/z values). Fig. 3 shows the evolution of products partition in the outlet mixture expressed in terms of flows of each compound. Due to the overlapping of the different m/z signals associated with hydrocarbons with the number of carbons $C_{n\geq 2}$ (see **Fig. S4**), C_2 and C_3 flow rates have been plotted without differentiating between alkanes, alkenes, or alkynes compounds (an estimation of the flow rates of C_2 and C_3 hydrocarbons is reported in **Table S4** in the Supplementary Material). Similar partitions of reactants in the outlet mixtures were obtained by other authors, such as Tu and Whitehead [19] or M. Kraus et al. [29], working with cylindrical packed-bed reactors filled with quartz wool.

A close look to Fig. 3 shows that *syngas* components (i.e., H_2 and CO) are majority products, followed by C_2 and C_3 hydrocarbons whose production is more noticeable at higher (i.e., 3:1 and 4:1) CH_4:CO_2 ratios. We conclude that the formation of C_2-C_3 hydrocarbons (mainly C_2H_6, C_2H_2 C_3H_8 and C_3H_6, see Supplementary Material **S4**) requires the

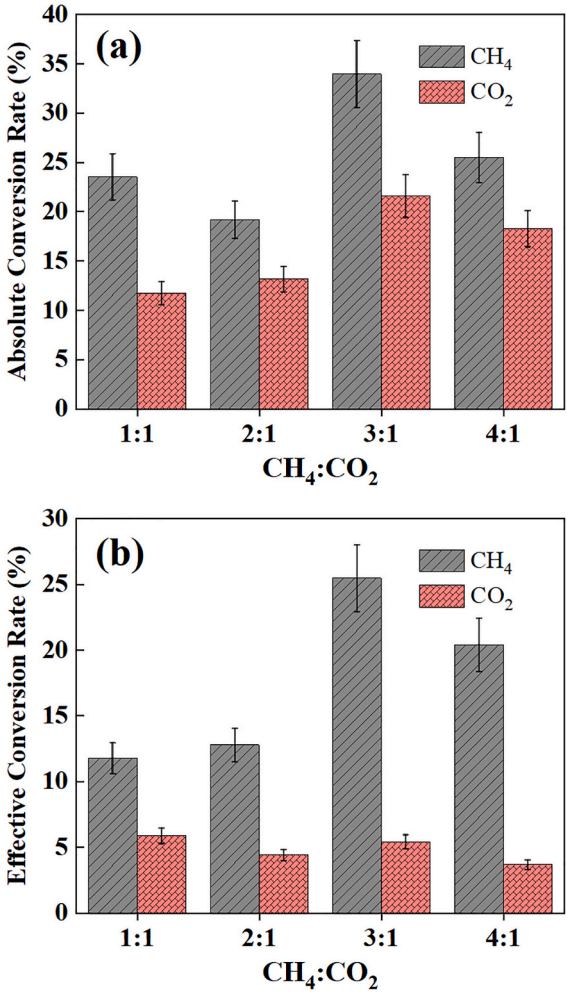

Fig. 2. (a) Absolute and (b) effective CH_4 and CO_2 conversion rates as a function of the CH_4:CO_2 ratio. Operating conditions: 5 mm-PZT barrier, total flow rate of 20 sccm, voltage amplitude of 3.15 kV, frequency of 5 kHz, and CH_4:CO_2 ratio varying between 1:1 and 4:1.

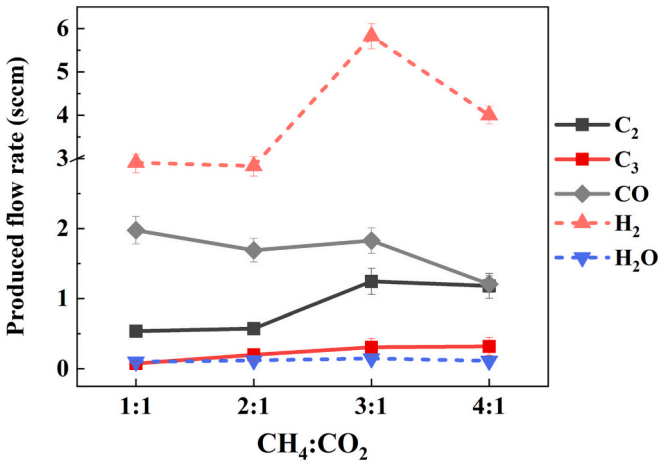

Fig. 3. Flow rates of the different reaction products as a function of the CH_4:CO_2 ratio. H_2 (pink) and H_2O (blue) flow rates are represented with dash lines, while C_2 hydrocarbons (black), C_3 hydrocarbons (red), and CO (gray) flow rates are represented in solid lines. The reported values are obtained from the QMS spectra in **Fig. S4**. (For interpretation of the references to colour in this figure legend, the reader is referred to the web version of this article.)

presence of a high amount of CH_4 in the discharge and, as it is indicated in Fig. 2, a higher power consumption. The produced amount of H_2 follows a similar tendency than the CH_4 conversion rate (c.f., Fig. 1) as expected from the fact that methane is the unique source of hydrogen atoms available in the system [19]. Flow rates of C_2 and C_3 hydrocarbons follow similar tendencies (i.e., reproduce the evolution of effective CH_4 conversion rates), although the amount of C_3 slightly varies from the 3:1 to the 4:1 mixture. At this point it is interesting to highlight the results of a semiquantitative comparison of the amount of H_2 produced vs. that of C_n hydrocarbons. These latter must be produced through reactions of the type:

$$nCH_4 \rightarrow C_nH_y + (4n - y)/2\ H_2 \quad \text{(E4)}$$

that entail a considerable formation of H_2. Assuming that most hydrocarbons are saturated, eq. *(E4)* means that the formation of one C_2 molecule would require two CH_4 molecules and will give rise to one H_2 molecule. A similar estimation can be done for C_3 and higher hydrocarbons. Note that these estimations would render even higher amounts of H_2 if unsaturated hydrocarbons are produced. According to these considerations and referring for simplicity to the data points for the 3:1 CH_4:CO_2 ratio in Fig. 3, the flow rates of C_2 (1.2 sscm) and C_3 (0.3 sscm) molecules would render a flux of hydrogen of ca. 1.8 sccm, i.e., a significant amount of the total detected H_2. Similar conclusions can be derived from the evaluation of data points for the other CH_4:CO_2 ratios in Fig. 3. Although we do not think that the comparison of the values as done here should be taken in absolute terms, it clearly demonstrates that an important source of hydrogen in the studied process are reactions such as *(E4)*.

Based on a similar reasoning basis, it is also of interest accounting for the formation of CO, the other component of the *syngas*-like mixture obtained in this process. The evolution of the CO flow follows the effective CO_2 conversion rate and the amount of CO_2 in the inlet mixture, i.e., it decreases with the CH_4:CO_2 reactant ratio. For the 3:1 ratio in Fig. 3, the flow of CO is 1.8 sccm, while the flow of decomposed CO_2, according to Fig. 2, renders a value of 1.1 sccm. This means that besides CO_2 splitting, carbon atoms coming from methane molecules also contribute to the formation CO. We propose that this formation occurs through the oxidation of solid carbon, which stemming from CH_4 decomposition becomes deposited on the pellets surface (as discussed in **section 3.3** below). Unlike this plasma/solid reaction, the interaction in the plasma of intermediate species stemming from CH_4 and CO_2 splitting is unlikely because oxygenated compounds, such as formaldehyde and acetaldehyde, were not detected in these experiments. In agreement with the previous hypothesis, O_2 was not detected as reaction product, while comparing the CO_2 conversion rate in Fig. 2 and the CO flows in Fig. 3 it is apparent that all oxygen coming from the converted CO_2 appears as CO (and minor amounts of H_2O molecules: 0.1 sccm for all studied ratios, c.f. Fig. 3). In other words, the CO flow in the reactant mixture is nearly twice the flow of converted CO_2 and roughly half of it must proceed from the oxidation of carbon deposits coming from CH_4.

The absence of oxygenates and our considerations above about the formation of C_2-C_3, H_2 and CO arise the question about the reaction mechanisms and the apparent lack of interaction between intermediate plasma species stemming from CO_2 and CH_4.

3.2. Intermediate plasma species and reaction mechanisms

Optical emission measurements provided interesting insights into the plasma-chemistry of the studied mixture. The OES spectra reported in Fig. 4 show that, for all operating conditions, bands corresponding to CH* excited species present maximum intensities. The most intense CH* band was found at 314 nm and can be ascribed to the $C^2\Sigma \rightarrow X^2\Pi$ system; in addition, a band corresponding to the $A^2\Delta \rightarrow X^2\Pi$ CH-system was also recorded at around 430 nm [42]. Similarly to other authors [19,29], bands attributed to the C_2 Swan system have been also detected at

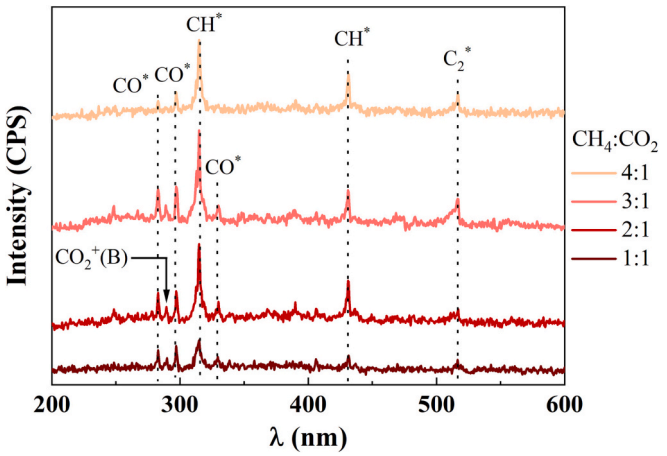

Fig. 4. Emission spectra acquired for the $CH_4 + CO_2$ plasmas. Main emission bands are indicated. Operating conditions: 5 mm-PZT barrier, total flow rate of 20 sccm, voltage amplitude of 3.15 kV, frequency of 5 kHz, and CH_4:CO_2 ratio varying between 1:1 and 4:1.

around 516 nm [42]. According to the literature, C_2 excited species may be formed during hydrocarbons degradation and can contribute to the formation of carbon deposits on the packed-bed and on the surface of the electrodes [5,9]. No significant contributions of OH* species (306 nm) can be observed in the spectra, a feature that, in agreement with other authors [19], is due the small amount of water found in the outlet mixture. Meanwhile, bands associated with the Third Positive System of CO are detected at 283.3, 297.7, and 313.4 nm, the latter overlapping the emission of CH* species at 314 nm. Finally, formation of $CO_2^+(B)$ states can be inferred by the detection of bands between 288.3 and 289.6 nm [37].

In addition to these bands, it is noticeable an increase in the spectral background at low wavelengths that can be attributed to the emission of H_2 excited species [43]. It is also interesting that the CO* bands present small intensities for the 4:1 mixture, a result agreeing with the lower flow of CO produced under these conditions.

To account for the detection by OES of CH* species as majority intermediate species, we propose the electron impact processes represented in eqs. *(E5)–(E7)* as reaction pathways for the dissociation of the CH_4 molecule:

$$CH_4 + e^- \rightarrow CH_3 + H + e^- \quad \text{(E5)}$$

$$CH_4 + e^- \rightarrow CH_2 + H_2 + e^- \quad \text{(E6)}$$

$$CH_4 + e^- \rightarrow CH + H_2 + H + e^- \quad \text{(E7)}$$

These processes are characterized by, respectively, threshold electron energies of 9, 10 and 12 eV and are expected to be highly dependent on the electron energy distribution function of electrons (EEDF) [19]. Reported simulations of electron impact interactions reveal that, working with dielectrics as DBD moderators, process *(E5)* accounts for ca. 80% of the electron impact dissociation of CH_4 [31,44]. As a result, C_2H_6 (i.e., CH_3-CH_3) and C_3H_8 (i.e., CH_3-CH_2-CH_3) are generally reported as typical hydrocarbons produced during $CO_2 + CH_4$ DBD plasma reactions [5]. Non-negligible amounts of C_2H_2 has been also detected in our experiment (see Supplementary Material **S4** and the relatively high intensity of the QMS peak at $m/z = 25$ in **Fig. S5**, mainly due to C_2H_2 [26]), very likely due to the direct association of CH* species produced in *(E7)* and detected by OES. The shift to higher energies of the characteristic EEDFs for our experimental configuration using PZT as discharge moderator [37] can justify a certain deviation from the typical pattern profile of hydrocarbons obtained with dielectrics as discharge moderators.

In addition to reactions *(E5)–(E7)* as electron impact reaction pathways for the production of C_2-C_3 hydrocarbons and H_2, the full decomposition of CH_4 into carbon and H_2 should be also mentioned as contributing to the overall formation of this gas. In fact, according to Tu and Whitehead [19], deposition of solid carbon can take place through the direct decomposition of CH_4 by reaction *(E8)*:

$$CH_4 + e^- \rightarrow C + 2H_2 + e^- \quad \text{(E8)}$$

This reaction has a threshold energy of 14 eV [19], generally too high for classic DBD configurations, but achievable when working with ferroelectrics in packed-bed reactors as in our experimental system. Some carbon deposition was in fact detected on the surface of PZT pellets after the experiments, as evidenced by XPS analysis of the pellets (see supplementary material, **Fig. S5**). The aforementioned detection of C_2* species in the plasma (cf., Fig. 4) is another hint suggesting that the complete dissociation of CH_4 into carbon and H_2 also occurs under our operating conditions.

The spectra in Fig. 4 also show the formation of CO* and CO_2^+ excited species in the plasma. In a previous study about plasma CO_2 splitting [37], we have found that these species are the main intermediates formed by electron impact activation of the CO_2 molecules, according to reactions of the type *(E9)–(E11)*:

$$CO_2 + e^- \text{ (high energy)} \rightarrow CO_2^+ \, (CO_2^{+*}) + 2e^- \quad \text{(E9)}$$

$$CO_2 + e^- \text{ (high energy)} \rightarrow CO^* + O + e^- \quad \text{(E10)}$$

$$CO_2^+ \, (CO_2^{+*}) + e^- \text{ (high energy)} \rightarrow CO^* + O \quad \text{(E11)}$$

According to them, reactive O radicals result from the electron impact excitation of CO_2. These highly reactive radicals are not detected by OES in our experiments and should be characterized by short lifetimes [3]. From a chemical point of view, these very reactive species might intervene in the reaction with methane and methane-derived radicals (i.e., *(E5)–(E7)*) to promote the formation of oxygenates. However, oxygenates are not observed under our working conditions, a result contradicting recent results by Biswas et al. [45], who using an isotope labelling technique to study $C_2H_6 + CO_2$ mixtures concluded that oxygenates formation involves the oxidation of ethane-derived species by O atoms stemming from CO_2. The reason why a similar process does not take place with methane is a question for debate that points to a distinct reactivity of the CH_x* species formed through reactions *(E6)–(E7)*. Nevertheless, oxygen radicals appear to effectively react with carbon deposits produced on the surface of the pellets, inducing their removal in form of CO_2, and, particularly, CO according to an Eley-Rideal (*E*-R) mechanisms as indicated in *(E12)*:

$$O \text{ (plasma)} + C(s) \rightarrow CO \text{ (plasma)} \quad \text{(E12)}$$

To prove the effectiveness of such a surface reaction process in the PZT-moderated packed-bed reactor with CH_4 and oxygen radicals, we carried out a specific experiment with a $CH_4 + O_2$ mixture (1 sccm O_2 and 16 sccm CH_4). The addition of oxygen to CH_4 enabled the stable ignition of the discharge (not possible in our reactor trying to ignite a pure-CH_4 flow due to short-circuiting because of the formation of considerable amounts of carbon) and a pattern distribution of products qualitatively similar to that found for the $CO_2 + CH_4$ mixtures (see supplementary material, **Fig. S6**). This result is compatible with the formation of hydrocarbons and carbon residues, as well as H_2, coming from CH_4, and the formation of CO by a reaction similar to *(E12)* where the active species of oxygen would proceed from O_2. For the $CH_4 + CO_2$ mixtures, oxygen atoms involved in reaction *(E12)* stem from CO_2 (reactions *(E9)–(E11)*) also contributing to the formation of CO and, less likely, CO_2. Notably, the carbon in the extra CO formed (actually stemming from CH_4 and not CO_2) will sum up to the CO formed by direct dissociation of CO_2.

3.3. Isotope labeling analysis with $^{13}CO_2$ as reactant in $CH_4 + CO_2$ mixtures

To further analyze the reaction mechanisms involved during the plasma activation of $CO_2 + CH_4$ mixtures, we applied the isotope labeling methodology using $^{13}CO_2$ instead of $^{12}CO_2$ as reactant. The experiment was performed for a 2:1 CH_4:CO_2 ratio, a total flow rate of 20 sccm, and similar electrical operating conditions than above (3.15 kV, 5 kHz). Fig. 5 illustrates the mass spectra acquired in the steady state after plasma ignition for mixtures with $^{12}CO_2$ (gray line) and $^{13}CO_2$ (red line). Fig. 5(a) shows the QMS spectra for *m/z* values from 0 to 100 in logarithmic scale. Peaks associated with H_2, H_2O, and CH_4 are located at the same positions for the two mixtures. Interestingly, signals associated to C_n hydrocarbons remain in the same position and depict similar intensities in the two cases, while a shift is detected between peaks at *m/z* = 28 and 29 and m/z = 44 and 45, depending on whether $^{12}CO_2$ and $^{13}CO_2$ are used for the experiments. Fig. 5(b) shows the zoomed *m/z* region between 24 and 46. The comparison of the plots with $^{12}CO_2$ or $^{13}CO_2$ in the reactant mixture clearly indicates that the flow of produced CO has only ^{12}C atoms in the former case and ^{12}C and ^{13}C atoms in the latter. Meanwhile, the hydrocarbon signals remain at the same position (i.e., these fragments only contain ^{12}C atoms from CH_4).

For the isotope-labeled mixture, contribution to m/z = 29 is due to ^{13}CO molecules, while the contribution to m/z = 28 must stem from ^{12}C atoms in ^{12}CO, C_2 and C_3 hydrocarbons and in the CH_4 molecules, coinciding with the peak pattern of these hydrocarbons when studying the $CH_4 + {}^{12}CO_2$ mixture. As expected, the CO_2 peaks appears at m/z = 44 and m/z = 45 for the $^{12}CO_2$ and the $^{13}CO_2$ mixtures, respectively.

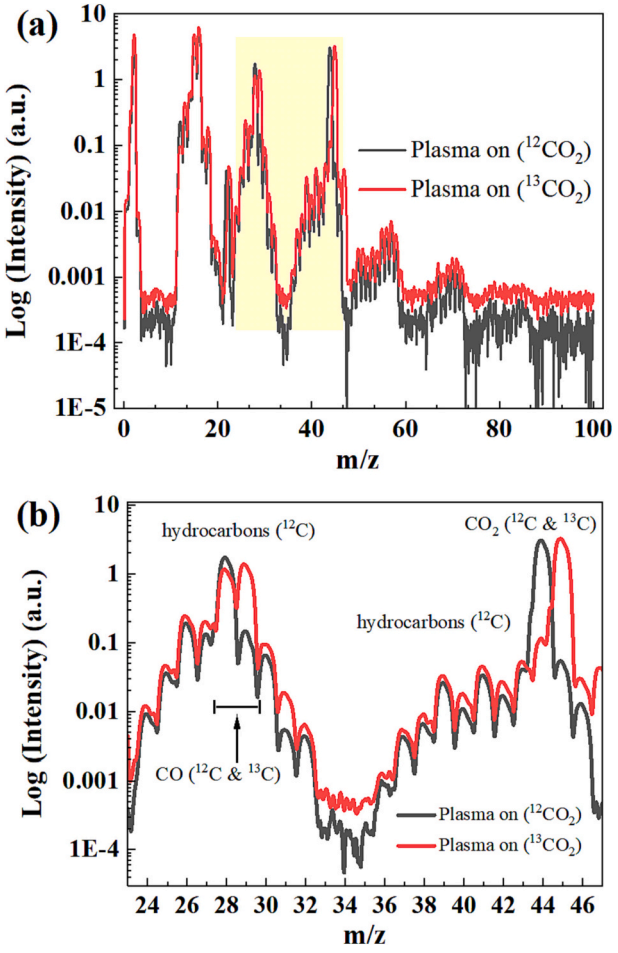

Fig. 5. QMS spectra in logarithmic scale acquired using $^{12}CO_2$ (gray line) and $^{13}CO_2$ (red line) for the 2:1 mixture. (a) General spectra, (b) Zoomed zone between m/z = 24 and m/z = 46. (For interpretation of the references to colour in this figure legend, the reader is referred to the web version of this article.)

These observations indicate that CH_4 and CO_2 follow nearly independent plasma reaction pathways in the gas phase leading to the formation of H_2 and hydrocarbons in the former and CO in the latter case. To some extent, we have proved here that there is also some CO coming from CH_4, in this case through the oxidation of carbon deposits formed by the complete decomposition of CH_4. According to our results, these independent plasma chemical routes only intersect following Eley-Rideal mechanisms to form CO and H_2O. The former is by no means a negligible process and contributes to around 47% of the produced CO flow rate for the 2:1 mixture, while the latter is minority (around 0.1 sccm of H_2O is produced, as indicated in Fig. 3). In this regard, the balance between the oxygen atoms that are able to react (coming from reacted CO_2) and those contained in the product flow rate (in the form of CO and H_2O) reveals that the formation of oxygenated compounds (CHO, CH_3OH, etc.) should be negligible. We represent this situation with the reaction scheme in Fig. 6, showing that main reaction products resulting from CH_4 are H_2 and hydrocarbons (mainly C_2 and C_3), as indicated in the upper zone of the scheme (blue arrows). Meanwhile, the direct dissociation of the CO_2 into O and CO is the dominant pathway for this molecule (bottom part of Fig. 6, brown arrows). Finally, the Eley-Rideal mechanisms between carbon deposits at the surface coming from CH_4 (without discarding a minority carbon coming from CO_2) and oxygen atoms in the plasma formed by CO_2 splitting is represented with a dash black line. Additionally, reactions in the gas phase between H_2 molecules (or H atoms) and O atoms should be taken as a minor reaction pathway to form H_2O (indicated with gray dash lines in Fig. 6).

This reaction scheme implies that no significant interaction occurs between O and CH_x species (including the stable CH_4 and the produced C_n hydrocarbons). Meanwhile, oxygen radicals appear to be quite effective in reacting with carbon deposits, similarly to their etching role in PECVD processes when hydrocarbons and CO_2 are used as precursor gases [33,34]. This lack of interaction between species formed along the two plasma pathways precludes the formation of oxygenates as reaction

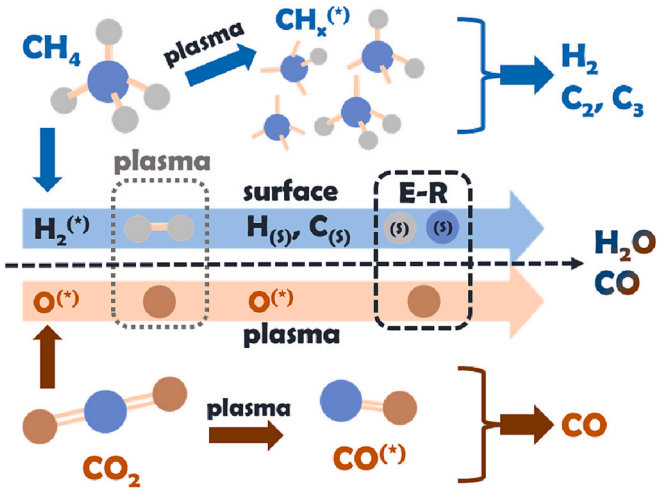

Fig. 6. Scheme of the independent plasma reaction pathways in the plasma phase and the cross-linked Eley-Rideal mechanisms for $CH_4 + CO_2$ mixtures. Solid blue arrows illustrate the plasma reaction pathways accounting for the production of H_2, C_2, C_3 hydrocarbons from CH_4, while solid brown arrows illustrate the formation of CO directly produced from CO_2. The dashed black line illustrates reaction pathways following Eley-Rideal mechanisms between oxygen plasma atoms and carbon deposits stemming from CH_4, producing CO, including also the possibility of reactions between oxygen and hydrogen to form H_2O. Plasma reactions between O atoms and H_2 are indicated with a dash gray line, considered to be a minor reaction pathway for H_2O production. (For interpretation of the references to colour in this figure legend, the reader is referred to the web version of this article.)

product, although explains well the formation of a *syngas*-like mixture (i.e., DRM process) and C_n hydrocarbons. At this point we can speculate that, to produce oxygenates, intermediate species from methane (i.e., CH_x*, H*) and CO_2 (i.e., CO*, O*, CO_2^+*) should interact through effective reaction pathways on the surface of a suitable catalyst present in the medium, either through Eley-Rideal (*E*-R) or Langmuir-Hinshelwood (L-H) reaction mechanisms. Metal catalysts have been recently claimed as a promising strategy to produce oxygenates from $CH_4 + CO_2$ mixtures [3]. For example, Ni has been proposed as a suitable candidate due to its capacity to dissociate methane at high temperatures [46]. Nevertheless, selection of suitable catalysts in the context of plasma-catalysis processes should not mimic their conventional use in thermal catalysis. In concrete for the $CO_2 + CH_4$ mixtures bifunctional catalysts should be desirable to, on the one hand, contribute to CO or CO_2 hydrogenation, and the other to the CH_4 dissociation on its surface. It is also noteworthy that the reaction scheme in Fig. 6 does not seem to apply for $C_2H_6 + CO_2$ mixtures where, as reported in the literature [45,47], oxygenates are effectively formed by plasma reaction. Whether this difference is due to distinct plasma reaction mechanisms because of the use of C_2H_6 instead of CH_4 or to the presence of dielectric oxides as catalysts in addition to ferroelectric moderators [47] or both, is an open question that requires additional investigation.

4. Conclusions

In this study, $CH_4 + CO_2$ mixtures have been investigated using a PZT-moderated packed-bed reactor operated at atmospheric pressure and ambient temperature. *Syngas*-like (CO and H_2), as well as C_2 and C_3 hydrocarbons (small amounts of C_4-C_6 hydrocarbons were also obtained for CH_4 rich mixtures) and minor amounts of H_2O were the main reaction products for CH_4:CO_2 ratios between 1:1 and 4:1. The CH_4 conversion rate was always higher than that of CO_2, a feature suggesting a certain decoupling of the decomposition processes of the two reactants. A direct insight into the reaction mechanisms by OES revealed the formation of CH*, CO*, CO_2* and C_2* excited species, the latter usually related to the deposition of carbon. We claim that this process is favored by the high-energy electrons existing in the PZT-moderated packed-bed reactor used in the present work. Again, the lack of any kind of OES signal attributable to $C_xH_yO_z$ intermediate species further supports the absence of crosslink interactions between plasma species stemming from CH_4 and CO_2. A direct proof in this line was obtained applying the isotope labeling methodology, using $^{13}CO_2$ instead of $^{12}CO_2$ in the $CH_4 + CO_2$ reaction mixture. Interestingly C_2 and C_3 hydrocarbons presented only ^{12}C in their structure, while carbon monoxide consisted of ^{13}CO and ^{12}CO. This evidence confirms that carbon atoms from CO_2 do not mix with hydrogen from CH_4 and that, therefore, the two reactants follow parallel plasma reaction pathways that do not significantly interact between them (apart from a minor possible interaction to render H_2O). The investigation of suitable catalysts promoting the interaction at the surface of CH_x* and CO*/ O* species is proposed as a research line to overcome the found restriction for the production of higher added value compounds by the plasma reaction of $CH_4 + O_2$ mixtures.

CRediT authorship contribution statement

Paula Navascués: Investigation, Formal analysis, Writing – original draft. **José Cotrino:** Conceptualization, Methodology, Supervision. **Agustín R. González-Elipe:** Conceptualization, Methodology, Supervision, Writing – review & editing. **Ana Gómez-Ramírez:** Formal analysis, Conceptualization, Methodology, Writing – review & editing, Supervision, Project administration, Funding acquisition.

Declaration of Competing Interest

The authors declare that they have no known competing financial interests or personal relationships that could have appeared to influence the work reported in this paper.

Data availability

Data will be made available on request.

Acknowledgments

The authors acknowledge projects PID2020-114270RA-I00, and PID2020-112620GB-I00 funded by MCIN/AEI/10.13039/501100011033, project TED2021-130124A-I00 funded by MICIN/AEI/10.13039/501100011033/Unión and Europea Next Generation EU/PRTR and projects P18-RT-3480, US-1381045, and US-1380977 funded by Consejería de Economía, Conocimiento, Empresas y Universidad de la Junta de Andalucía (PAIDI-2020) and Programa Operativo Feder 2014-2020. The authors also would like to thank F. Vattier Lagarrigue from the Materials Science Institute of Sevilla for her support with XPS measurements.

Appendix B. Supplementary data

The supplementary material includes: (S1) photographs of the packed-bed reactor and its components, (S2) scheme of the parallel plate packed-bed reactor and the electrical excitation & diagnosis system, (S3) sketch of the connections between the reactor and the characterization techniques, (S4) mass spectra recorded for the different $CO_2 + CH_4$ mixtures and estimation of the produced flow rates of C_2 and C_3 hydrocarbons, (S5) XPS analysis of PZT pellets before and after their use as moderators in $CH_4 + CO_2$ discharges, and (S6) QMS spectra recorded for the $CH_4 + O_2$ mixture. Supplementary data to this article can be found online at https://doi.org/10.1016/j.fuproc.2023.107827.

References

[1] R.W. Howarth, R. Santoro, A. Ingraffea, R.W. Howarth, R. Santoro, A. Ingraffea, Methane and the greenhouse-gas footprint of natural gas from shale formations, Clim. Chang. 106 (4) (2011) 679–690, https://doi.org/10.1007/S10584-011-0061-5.
[2] H. Puliyalil, D. Lašič Jurković, V.D.B.C. Dasireddy, B. Likozar, A review of plasma-assisted catalytic conversion of gaseous carbon dioxide and methane into value-added platform chemicals and fuels, RSC Adv. 8 (2018) 27481–27508, https://doi.org/10.1039/c8ra03146k.
[3] S. Liu, L.R. Winter, J.G. Chen, Review of plasma-assisted catalysis for selective generation of oxygenates from CO_2 and CH_4, ACS Catal. 10 (2020) 2855–2871, https://doi.org/10.1021/acscatal.9b04811.
[4] E.V. Kondratenko, T. Peppel, D. Seeburg, V.A. Kondratenko, N. Kalevaru, A. Martin, S. Wohlrab, Methane conversion into different hydrocarbons or oxygenates: current status and future perspectives in catalyst development and reactor operation, Catal, Sci. Technol. 7 (2017) 366–381, https://doi.org/10.1039/C6CY01879C.
[5] R. Snoeckx, A. Bogaerts, Plasma technology-a novel solution for CO_2 conversion? Chem. Soc. Rev. 46 (2017) 5805–5863, https://doi.org/10.1039/c6cs00066e.
[6] W. Taifan, J. Baltrusaitis, CH_4 conversion to value added products: potential, limitations and extensions of a single step heterogeneous catalysis, Appl. Catal. B. 198 (2016) 525–547, https://doi.org/10.1016/J.APCATB.2016.05.081.
[7] A. Fridman, Plasma chemistry, Plasma Chem. 9780521847353 (2008) 1–978, https://doi.org/10.1017/CBO9780511546075.
[8] A. Lebouvier, S.A. Iwarere, P. D'Argenlieu, D. Ramjugernath, L. Fulcheri, Assessment of carbon dioxide dissociation as a new route for syngas production: a comparative review and potential of plasma-based technologies, Energy Fuel 27 (2013) 2712–2722, https://doi.org/10.1021/EF301991D.
[9] W.C. Chung, M.B. Chang, Review of catalysis and plasma performance on dry reforming of CH4 and possible synergistic effects, Renew. Sust. Energ. Rev. 62 (2016) 13–31, https://doi.org/10.1016/j.rser.2016.04.007.
[10] X. Wang, S. Xu, W. Yang, X. Fan, Q. Pan, H. Chen, Development of Ni-Co supported on SBA-15 catalysts for non-thermal plasma assisted co-conversion of CO_2 and CH_4: results and lessons learnt, Carb. Capt. Sci. Technol. 5 (2022), 100067, https://doi.org/10.1016/j.ccst.2022.100067.
[11] M.S. Cha, R. Snoeckx, Plasma technology–preparing for the electrified future, Front. Mech. Eng. 8 (2022) 45, https://doi.org/10.3389/FMECH.2022.903379/BIBTEX.
[12] I. Michielsen, Y. Uytdenhouwen, A. Bogaerts, V. Meynen, Altering conversion and product selectivity of dry reforming of methane in a dielectric barrier discharge by changing the dielectric packing material, Catalysts 9 (2019) 51, https://doi.org/10.3390/CATAL9010051.

[13] Y. Zeng, X. Zhu, D. Mei, B. Ashford, X. Tu, Plasma-catalytic dry reforming of methane over γ-Al2O3 supported metal catalysts, Catal. Today 256 (2015) 80–87, https://doi.org/10.1016/J.CATTOD.2015.02.007.

[14] W.C. Chung, K.L. Pan, H.M. Lee, M.B. Chang, Dry reforming of methane with dielectric barrier discharge and ferroelectric packed-bed reactors, Energy Fuel 28 (2014) 7621–7631, https://doi.org/10.1021/ef5020555.

[15] X. Tu, H.J. Gallon, M.V. Twigg, P.A. Gorry, J.C. Whitehead, Dry reforming of methane over a Ni/Al_2O_3 catalyst in a coaxial dielectric barrier discharge reactor, J. Phys. D. Appl. Phys. 44 (2011), https://doi.org/10.1088/0022-3727/44/27/274007.

[16] Y. Li, C.J. Liu, B. Eliasson, Y. Wang, Synthesis of oxygenates and higher hydrocarbons directly from methane and carbon dioxide using dielectric-barrier discharges: product distribution, Energy Fuel 16 (2002) 864–870, https://doi.org/10.1021/ef0102770.

[17] A. Bogaerts, C. de Bie, R. Snoeckx, T. Kozák, Plasma based CO_2 and CH_4 conversion: a modeling perspective, Plasma Process. Polym. 14 (2017), https://doi.org/10.1002/ppap.201600070.

[18] A. Majumdar, F. Behnke, R. Hippler, K. Matyash, R. Schneider, Chemical Reaction Studies in CH_4 /Ar and CH_4 /N_2 Gas mixtures of a dielectric barrier discharge, J. Phys. Chem. A (2005) 9371–9377, https://doi.org/10.1021/jp053588a.

[19] X. Tu, J.C. Whitehead, Plasma-catalytic dry reforming of methane in an atmospheric dielectric barrier discharge: understanding the synergistic effect at low temperature, Appl. Catal. B. 125 (2012) 439–448, https://doi.org/10.1016/J.APCATB.2012.06.006.

[20] Y. Li, C.J. Liu, B. Eliasson, Y. Wang, Synthesis of oxygenates and higher hydrocarbons directly from methane and carbon dioxide using dielectric-barrier discharges: product distribution, Energy Fuel 16 (2002) 864–870, https://doi.org/10.1021/EF0102770.

[21] L.M. Martini, G. Dilecce, G. Guella, A. Maranzana, G. Tonachini, P. Tosi, Oxidation of CH_4 by CO_2 in a dielectric barrier discharge, Chem. Phys. Lett. 593 (2014) 55–60, https://doi.org/10.1016/J.CPLETT.2013.12.069.

[22] A. Ozkan, T. Dufour, G. Arnoult, P. de Keyzer, A. Bogaerts, F. Reniers, CO_2-CH_4 conversion and syngas formation at atmospheric pressure using a multi-electrode dielectric barrier discharge, J. CO2 Utiliz. 9 (2015) 74–81, https://doi.org/10.1016/j.jcou.2015.01.002.

[23] M. Scapinello, L.M. Martini, P. Tosi, CO_2 hydrogenation by CH_4 in a dielectric barrier discharge: catalytic effects of nickel and copper, Plasma Process. Polym. 11 (2014) 624–628, https://doi.org/10.1002/PPAP.201400023.

[24] A.J. Zhang, A.M. Zhu, J. Guo, Y. Xu, C. Shi, Conversion of greenhouse gases into syngas via combined effects of discharge activation and catalysis, Chem. Eng. J. 156 (2010) 601–606, https://doi.org/10.1016/J.CEJ.2009.04.069.

[25] L. Wang, Y. Yi, C. Wu, H. Guo, X. Tu, One-step reforming of CO_2 and CH_4 into high-value liquid chemicals and fuels at room temperature by plasma-driven catalysis, Angew. Chem. Int. Ed. 56 (2017) 13679–13683, https://doi.org/10.1002/ANIE.201707131.

[26] V.J. Rico, J.L. Hueso, J. Cotrino, A.R. González-Elipe, Evaluation of different dielectric barrier discharge plasma configurations as an alternative technology for green C1 chemistry in the carbon dioxide reforming of methane and the direct decomposition of methanol†, J. Phys. Chem. A 114 (2010) 4009–4016, https://doi.org/10.1021/JP100346Q.

[27] K. Zhang, T. Mukhriza, X. Liu, P.P. Greco, E. Chiremba, A study on CO_2 and CH_4 conversion to synthesis gas and higher hydrocarbons by the combination of catalysts and dielectric-barrier discharges, Appl. Catal. A Gen. 502 (2015) 138–149, https://doi.org/10.1016/J.APCATA.2015.06.002.

[28] X. Zheng, S. Tan, L. Dong, S. Li, H. Chen, $LaNiO_3$@SiO_2 core–shell nano-particles for the dry reforming of CH_4 in the dielectric barrier discharge plasma, Int. J. Hydrog. Energy 39 (2014) 11360–11367, https://doi.org/10.1016/J.IJHYDENE.2014.05.083.

[29] M. Kraus, W. Egli, K. Haffner, B. Eliasson, U. Kogelschatz, A. Wokaun, Investigation of mechanistic aspects of the catalytic CO_2 reforming of methane in a dielectric-barrier discharge using optical emission spectroscopy and kinetic modeling, Phys. Chem. Chem. Phys. 4 (2002) 668–675, https://doi.org/10.1039/b108040g.

[30] R. Snoeckx, R. Aerts, X. Tu, A. Bogaerts, Plasma-based dry reforming: a computational study ranging from the nanoseconds to seconds time scale, J. Phys. Chem. C 117 (2013) 4957–4970, https://doi.org/10.1021/JP311912B/SUPPL_FILE/JP311912B_SI_001.PDF.

[31] C. de Bie, Fluid Modeling of the Plasma-Assisted Conversion of Greenhouse Gases to Value-Added Chemicals in a Dielectric Barrier Discharge, University of Antwerp, 2016.

[32] W. Wang, R. Snoeckx, X. Zhang, M.S. Cha, A. Bogaerts, Modeling plasma-based CO_2 and CH_4 conversion in mixtures with N_2, O_2, and H_2O: the bigger plasma chemistry picture, J. Phys. Chem. C 122 (2018) 8704–8723, https://doi.org/10.1021/acs.jpcc.7b10619.

[33] D. Hegemann, U. Schütz, E. Körner, Macroscopic approach to plasma polymerization using the concept of energy density, Plasma Process. Polym. 8 (2011) 689–694, https://doi.org/10.1002/ppap.201000211.

[34] D. Hegemann, E. Körner, K. Albrecht, U. Schütz, S. Guimond, Growth mechanism of oxygen-containing functional plasma polymers, Plasma Process. Polym. 7 (2010) 889–898, https://doi.org/10.1002/ppap.200900144.

[35] R. Reuter, K. Rügner, D. Ellerweg, T. de Los Arcos, A. von Keudell, J. Benedikt, The role of oxygen and surface reactions in the deposition of silicon oxide like films from HMDSO at atmospheric pressure, Plasma Process. Polym. 9 (2012) 1116–1124, https://doi.org/10.1002/ppap.201100146.

[36] A. Gómez-Ramírez, J. Cotrino, R.M. Lambert, A.R. González-Elipe, Efficient synthesis of ammonia from N_2 and H_2 alone in a ferroelectric packed-bed DBD reactor, Plasma Sources Sci. Technol. 24 (2015), https://doi.org/10.1088/0963-0252/24/6/065011.

[37] P. Navascués, J. Cotrino, A.R. González-Elipe, A. Gómez-Ramírez, Plasma assisted CO_2 dissociation in pure and gas mixture streams with a ferroelectric packed-bed reactor in ambient conditions, Chem. Eng. J. 430 (2022), https://doi.org/10.1016/j.cej.2021.133066.

[38] A.M. Montoro-Damas, J.J. Brey, M.A. Rodríguez, A.R. González-Elipe, J. Cotrino, Plasma reforming of methane in a tunable ferroelectric packed-bed dielectric barrier discharge reactor, J. Power Sources 296 (2015) 268–275, https://doi.org/10.1016/j.jpowsour.2015.07.038.

[39] A.V. Pipa, R. Brandenburg, The equivalent circuit approach for the electrical diagnostics of dielectric barrier discharges: the classical theory and recent developments, Atoms. 7 (2019), https://doi.org/10.3390/atoms7010014.

[40] National Institute of Standards and Technology (NIST), Mass Spectrometer Data Center (n.d.), https://chemdata.nist.gov/ (accessed January 31, 2023).

[41] H. Höft, M.M. Becker, M. Kettlitz, R. Brandenburg, Upscaling from single- to multi-filament dielectric barrier discharges in pulsed operation, J. Phys. D. Appl. Phys. 55 (2022), 424003, https://doi.org/10.1088/1361-6463/AC868B.

[42] R.W.B. Pearse, A.G. Gaydon, The Identification of Molecular Spectra, 3rd ed., Chapman & Hall, London, 1965.

[43] K. Stapelmann, J.W. Lackmann, I. Buerger, J.E. Bandow, P. Awakowicz, A H_2 very high frequency capacitively coupled plasma inactivates glyceraldehyde 3-phosphate dehydrogenase(GapDH) more efficiently than UV photons and heat combined, J. Phys. D. Appl. Phys. 47 (2014), 085402, https://doi.org/10.1088/0022-3727/47/8/085402.

[44] C. de Bie, B. Verheyde, T. Martens, J. van Dijk, S. Paulussen, A. Bogaerts, Fluid modeling of the conversion of methane into higher hydrocarbons in an atmospheric pressure dielectric barrier discharge, Plasma Process. Polym. 8 (2011) 1033–1058, https://doi.org/10.1002/PPAP.201100027.

[45] A.N. Biswas, L.R. Winter, B. Loenders, Z. Xie, A. Bogaerts, J.G. Chen, Oxygenate production from plasma-activated reaction of CO_2 and ethane, ACS Energy Lett. 7 (2022) 236–241, https://doi.org/10.1021/acsenergylett.1c02355.

[46] J. Ashok, M.H. Wai, S. Kawi, Nickel-based catalysts for high-temperature water gas shift reaction-methane suppression, ChemCatChem. 10 (2018) 3927–3942, https://doi.org/10.1002/CCTC.201800031.

[47] A. Gómez-Ramírez, V.J. Rico, J. Cotrino, A.R. González-Elipe, R.M. Lambert, Low temperature production of formaldehyde from carbon dioxide and ethane by plasma-Assisted catalysis in a ferroelectrically moderated dielectric barrier discharge reactor, ACS Catal. 4 (2014) 402–408, https://doi.org/10.1021/cs4008528.